Research Square

Preprints are preliminary reports that have not undergone peer review.
They should not be considered conclusive, used to inform clinical practice,
or referenced by the media as validated information.

# A unimolecular GLP-1 and FGF21 dual agonist for treatment of metabolic dysfunction-associated steatohepatitis

**Ashutosh Chilkoti**

chilkoti@duke.edu

Duke University https://orcid.org/0000-0003-1301-1836

**Parul Sirohi**

Duke University

**Seh Hoon Oh**

Duke University

**Catherine Price**

Duke University

**Caslin Gilroy**

Duke University

**Joy Tong**

Duke University

**Huaxia Cui**

Duke University

**Danhong Lu**

Duke University

**Rajesh Dutta**

Duke University

**Anna Mae Diehl**

Duke University https://orcid.org/0000-0003-1859-089X

**Article**

**Keywords:** GLP-1, FGF21, Elastin-Like-Polypeptide (ELP), MASH

**Posted Date:** September 11th, 2025

**DOI:** https://doi.org/10.21203/rs.3.rs-7282812/v1

**License:** This work is licensed under a Creative Commons Attribution 4.0 International License.
Read Full License

**Additional Declarations:** There is **NO** Competing Interest.

---

**Version of Record:** A version of this preprint was published at Communications Medicine on June 11th, 2026. See the published version at https://doi.org/10.1038/s43856-026-01712-5.

# Abstract

We report the design and preclinical evaluation of a unimolecular dual agonist, GLP1-ELP-FGF21 (GEF), which integrates GLP-1 and FGF21 signaling by linking GLP-1 and FGF21 through a thermally responsive elastin-like polypeptide (ELP) linker. GEF was engineered for optimal receptor engagement and extended pharmacokinetics through reversible phase separation into a depot upon subcutaneous injection. GEF retained potent *in vitro* activity at both GLP-1R and FGFR1/β-Klotho pathways and demonstrated robust metabolic and hepatic benefits in a diet-induced murine model of advanced MASH. Treatment with GEF significantly reduced body weight, liver mass, serum glucose levels, and total cholesterol, while also attenuating hepatic inflammation and fibrosis. Molecular and histological analyses revealed suppressed expression of pro-fibrotic and inflammatory genes, reduced steatosis, and enhanced hepatocyte proliferation. Collectively, these findings establish GEF as a promising single-agent, multi-pathway therapeutic for treating advanced MASH.


# Introduction

Metabolic Dysfunction-Associated Steatohepatitis (MASH) has become a major global health challenge due to its increasing prevalence and association with liver-related complications, including cirrhosis and hepatocellular carcinoma [1]. Histologically, MASH is characterized by steatosis, hepatocyte ballooning, lobular inflammation, and varying degrees of fibrosis, which is the strongest predictor of long-term outcomes such as liver failure and mortality [2]. Despite the recent approval of Rezdiffra (resmetirom), which marks a significant milestone as the first FDA-approved therapy for non-cirrhotic MASH with moderate to advanced fibrosis, there remains a pressing clinical need for additional therapeutic options. MASH is a multifactorial disease characterized by metabolic dysfunction, inflammation, hepatocellular injury, and progressive fibrosis—components that may not be fully addressed by a single pathway-targeting agent. Rezdiffra primarily acts by reducing hepatic fat via thyroid hormone receptor activation [3], but it does not directly target fibrosis reversal or promote liver regeneration [4]. Moreover, patient heterogeneity, varied disease progression rates, and potential comorbidities highlight the need for multi-targeted or combination approaches [5]. Therefore, the development of next-generation therapeutics that can simultaneously modulate multiple pathological processes is urgently needed to more comprehensively treat MASH and prevent progression to cirrhosis or liver failure.

Glucagon-like peptide-1 (GLP-1) receptor agonists, originally developed to treat type 2 diabetes, have shown beneficial effects in MASH patients due to their ability to reduce body weight, improve insulin sensitivity, and decrease hepatic steatosis [6]. These agents exert their metabolic effects primarily through appetite suppression and delayed gastric emptying, resulting in reduced caloric intake and improved glycemic control [7]. While clinical trials of GLP-1 analogs like liraglutide and semaglutide have reported histological improvements in steatohepatitis, their ability to regress established fibrosis has been modest [2]. This limitation has prompted the search for complementary agents that more directly target fibrogenesis.

Fibroblast growth factor-21 (FGF21) is a hormone-like protein produced primarily by the liver in response to metabolic stress [8, 9]. It plays a central role in regulating lipid oxidation, ketogenesis, and insulin sensitivity, and has demonstrated therapeutic potential in both preclinical and early clinical studies of MASH [10, 11]. Importantly, FGF21 has also been shown to reduce liver inflammation and fibrosis independently of its metabolic effects, possibly through direct action on hepatic stellate cells and anti-inflammatory signaling pathways. Given the overlapping yet distinct actions of GLP-1 and FGF21, combining them into a single molecule offers a promising strategy for treating MASH [12]. We hence hypothesized that a unimolecular GLP1–FGF21 dual agonist may achieve more robust and coordinated control over metabolic, inflammatory, and fibrotic disease drivers while simplifying dosing and improving adherence compared to co-administration of individual agents [13].

To construct the unimolecular GLP1-FGF21 dual agonist, we use an elastin-like polypeptide (ELP)—a repetitive sequence of VPGXG, where X is any amino acid except Proline—as a linker between the GLP-1 and FGF21 domains [14]. We chose an ELP to link GLP-1 with − 21 for several reasons: 1) ELPs are intrinsically disordered polypeptides, which make them flexible linkers that should allow GLP-1 and FGF21 to engage with their respective receptors; 2) ELPs exhibit LCST phase behavior, such that they can be designed—at their sequence level—to be soluble in the syringe at room temperature, but undergo thermally driven phase separation into an insoluble coacervate depot upon subcutaneous (s.c.) injection, driven by body heat [15, 16]; 3) the kinetics of dissolution of the depot can be programmed by control of the hydrophobicity of the ELP sequence and its molecular weight [17, 18]; and 4) upon dissolution of the depot, the soluble GEF molecules released from the depot will have an extended circulation half-life compared to the individual drugs. These unique features make ELPs attractive for the design of a long-acting protein therapeutics [19].

Numerous mouse models have been developed to replicate various features of human MASH, including dietary models such as the methionine- and choline-deficient (MCD) diet, the Western diet (high in fat, cholesterol, and sugars), and genetic models like ob/ob and foz/foz mice [19]. However, many of these models either fail to develop significant fibrosis or confound the analysis of fibrosis by introducing obesity and insulin resistance as major variables. In this study, we utilized 24-week-old mice and fed them a choline-deficient, L-amino acid-defined high-fat diet (CDA-HFD) for 16 continuous weeks, which reliably induces advanced hepatic fibrosis while avoiding the confounding metabolic phenotypes seen in obesity or diabetes [20]. We choose this animal model because both the GLP-1R agonists and FGF21 are known to correct systemic metabolic dysfunction but their effect on MASH in absence of obesity and type-2 diabetes is unknown. Hence, this approach enabled a focused assessment of antifibrotic activity of GLP1-FGF21 dual agonist in a model that closely reflects advanced human MASH pathology but lacks metabolic abnormalities.

## Results and discussion

To generate a long-acting dual agonist capable of activating both GLP-1 and FGF21 pathways, we designed a single fusion protein incorporating active GLP-1 at the N-terminus, followed by an elastin-like

polypeptide (ELP) linker, and FGF21 at the C-terminus—hereafter referred to as **GEF** (**G**LP1-**E**LP-**F**GF21). We fused the C-terminus of GLP-1 to the ELP and the C-terminus of ELP was fused to FGF21 at its N-terminus terminus because this configuration preserved the receptor-binding capabilities of each hormone, while the linear design facilitated efficient production of the fusion protein in a bacterial expression system [13]. To enhance translational efficiency in *E. coli*, a leader sequence (MSKGPG) was added upstream of GLP-1 [21, 22]. Because GLP-1 requires a free N-terminus for bioactivity, a Tobacco Etch Virus (TEV) protease recognition site was inserted between the leader and the GEF sequence [23]. Following protein purification, the leader was cleaved by TEV protease, leaving a glycine residue. The remaining Gly-Ala (GA) dipeptide then serves as a substrate for endogenous Dipeptidyl peptidase 4 (DPP4), which cleaves after alanine, yielding a scarless and bioactive N-terminus on GEF [24] (Fig. 1A). This approach allowed for high-yield production of the fully functional fusion construct and the purified protein exhibited the expected molecular weight of 72 kDa, as confirmed by sodium dodecyl sulfate polyacrylamide gel electrophoresis (SDS-PAGE) (Fig. 1B), indicating successful expression and purification of the GEF fusion protein without major degradation products.

A critical design element of GEF is the inclusion of the ELP linker, which beyond linking the two proteins, imparts temperature-sensitive phase behavior to the fusion protein. The ELP sequence in the GEF protein was strategically selected for the fusion protein to exhibit a transition temperature ($T_t$) below body temperature. The thermal phase behavior of GEF was characterized by measuring its absorbance while gradually heating the protein solution. The temperature at which a sharp increase in turbidity was observed is defined as the $T_t$, and is consistent with the LCST phase behavior of ELPs [25]. We measured the $T_t$—defined as the temperature at the inflection point of the absorbance versus temperature curves—as a function of GEF concentration, and observed that the $T_t$ increased with decreasing protein concentration, which is consistent with the behavior of ELPs and their fusion proteins in the dilute and semi-dilute regime of their phase diagram [17, 18, 25] (Fig. 1C). Brightfield microscopy revealed that GEF undergoes phase separation into two immiscible phases—a dense phase of micron-size liquid droplets enriched in GEF and a dilute phase depleted in GEF—above its $T_t$ that readily dissolve into single phase upon cooling the protein below its $T_t$ (Fig. 1D). This phase transition behavior imparted by the ELP linker to GEF creates a depot upon subcutaneous (*s.c.*) administration but also enhances systemic circulation half-life by reducing renal clearance because of the increased molecular weight provided by the size of the ELP linker—two pharmacokinetic advantages that are critical for therapeutic efficacy of protein-based biologics.

To verify that both arms of the fusion protein retain bioactivity, we carried out pathway-specific *in vitro* cell-based activity assays. We used a HEK293 cell line that stably expresses GLP-1 receptor (GLP-1R) and a cAMP-responsive luciferase reporter to test the activity of the GLP-1 arm of the dual agonist [26]. GEF demonstrated robust activation of the GLP-1R, as seen by the dose-dependent increase in luminescence levels corresponding to the intracellular cAMP level, with an $EC_{50}$ of 2.2 ± 0.3 nM (Fig. 1E). We ran another potent GLP-1R agonist—Exendin-4—in the same assay as a positive control, and as expected, the activity of the GEF fusion protein was lower compared to Exendin-1 due to the steric

hinderance posed by the large molecule—an effect we have previously seen with other ELP fusion proteins [16, 26]. Separately, to test the activity of the FGF21 arm of the dual agonist, we utilized an engineered HEK293 cell line co-expressing FGFR1 and β-Klotho—the canonical receptor complex for FGF21 [22]. GEF activated the FGF21 signaling axis in a dose-dependent manner [18], as shown by phosphorylation of ERK1/2 with an $EC_{50}$ of 10 ± 4 nM (Fig. 1F). The signaling magnitude of GEF was only 10-fold lower as compared to the receptor activation by recombinant mouse FGF21 consistent with the effect of steric hindrance, and confirms that the C-terminal FGF21 domain in GEF is correctly folded and functional. Together, these in vitro findings establish that GEF is a bifunctional fusion protein with bioactivity for both GLP-1 and FGF21 receptors and that it exhibits phase transition behavior typical of ELPs.

To evaluate the therapeutic efficacy of the unimolecular dual agonist in a model of advanced MASH, we employed a chronic dietary induction protocol using 24-week-old C57Bl/6J mice. Animals were placed on a choline-deficient, high-fat diet (CDA-HFD) for 16 weeks, a well-established model that drives steatohepatitis and hepatic fibrosis in the absence of obesity. After 12 weeks of diet-induced liver injury, mice were randomized into two groups and administered either saline or GEF at a dose of 750 nmol/kg once weekly by s.c. injection over the final 4 weeks of the diet period (Fig. 2A). Body weight was recorded daily, and animals were euthanized at week 17 for liver and serum collection. Despite the advanced disease state at the onset of treatment, GEF administration led to a consistent reduction in body weight with each injection over the period of treatment, whereas saline-treated controls maintained their weight (Fig. 2B). This reduction in weight occurred without any observable signs of toxicity or stress and was driven by the central and peripheral metabolic effects of GLP-1R activation, as has been well documented in previous studies [13]. The observation that GEF retains the anorectic and weight-lowering activity of GLP-1 *in vivo* further validates the functional integrity of the GLP-1 moiety in the fusion construct.

In addition to reducing body weight, GEF treatment had a marked effect on liver mass. The liver-to-body weight ratio—an indirect indicator of hepatic steatosis and inflammation—was significantly lower in GEF-treated mice compared to controls at the end of the 16-week study (Fig. 2C). The observed reduction in relative liver weight likely reflects the combined effects of FGF21-mediated improvements in lipid metabolism and GLP-1-driven modulation of systemic energy balance [27]. The observed reductions in body and liver weight after just four weeks of treatment demonstrate that GEF produces sustained metabolic improvements and underscore the potential for this dual agonist to modulate key disease features in a mouse model of diet-induced MASH with advanced liver injury.

To further evaluate the potential of GEF on systemic metabolism, we performed serum biomarker analysis at the end of the 16-week study period by quantifying the circulating levels of total cholesterol, high density lipoprotein (HDL), insulin, and glucose in each animal. Mice treated with GEF exhibited significantly lower levels of total cholesterol compared to the saline controls (Fig. 3A), suggesting improved lipid handling and reduced hepatic lipid accumulation. Interestingly, HDL cholesterol levels were significantly higher in the GEF group, which is often considered cardioprotective [28] (Fig. 3B). GEF

treatment also produced notable effects on glucose homeostasis, as serum insulin levels were significantly higher, and glucose levels were significantly lower in GEF-treated animals as compared to the controls (Fig. 3C-D). The combined actions of GLP-1 and FGF21 within a single molecular entity appear to act cooperatively in reducing lipid burden, improving glycemic control, and restoring endocrine balance. These metabolic benefits provide a mechanistic basis for the observed reductions in liver pathology and body weight and support the therapeutic promise of GEF for multifactorial diseases like MASH, where multiple physiological pathways must be targeted simultaneously.

To investigate the impact of GEF treatment on hepatic inflammation and fibrosis—two hallmarks of MASH progression—we analyzed the expression of pro-fibrotic and pro-inflammatory genes in liver tissue using quantitative reverse transcription polymerase chain reaction (qRT-PCR). Gene expression analysis revealed that TGF-β—a central mediator of fibrogenesis and hepatic stellate cell activation—was significantly downregulated in livers of GEF-treated mice compared to saline controls (Fig. 4A). This reduction suggests a direct anti-fibrotic effect of the dual agonist, consistent with the known capacity of FGF21 to suppress stellate cell activation and collagen deposition [29]. In parallel, transcripts for key inflammatory cytokines—including TNFα, IL-6, IL-18, and IL-33—were decreased in the GEF group as compared to the saline group (Fig. 4B–E). These markers are associated with hepatic macrophage infiltration and innate immune activation, both of which contribute to liver injury and fibrotic remodeling in MASH [30]. The concurrent reduction across multiple cytokines suggests that GEF broadly suppresses hepatic inflammatory signaling, possibly through combined GLP-1–mediated modulation of immune cells and FGF21-driven hepatoprotection. To validate these transcriptional findings at the protein level, we also measured IL-6 protein concentrations in liver lysates by ELISA. Consistent with the gene expression data, IL-6 protein levels were significantly lower in GEF-treated animals (Fig. 4G), confirming that the transcriptional changes translate into protein, and reinforcing the anti-inflammatory effect of the treatment. Interestingly, expression of HIF1α—a transcription factor upregulated under hypoxic and inflammatory conditions and implicated in fibrogenic progression —was also slightly lower in the livers of GEF-treated animals (Fig. 4F). This downregulation further supports the notion that GEF improves the hepatic microenvironment, potentially reducing oxygen stress and limiting downstream activation of fibrotic pathways.

Beyond mitigating inflammation and fibrosis, a critical goal in the treatment of MASH is to promote hepatic repair and restore normal liver function. To evaluate whether GEF exerts pro-regenerative or hepatoprotective effects, we analyzed the expression of key genes involved in hepatocyte identity, liver regeneration, and cell cycle progression by qRT-PCR.

We first assessed hepatic mRNA levels of HNF4α—a master transcription factor essential for maintaining hepatocyte differentiation and liver-specific gene expression. GEF-treated mice showed a significant increase in HNF4α expression compared to controls (Fig. 5A), suggesting that the dual agonist may help preserve or restore hepatocellular identity in the diseased liver [31]. This is particularly important in the context of MASH, where hepatocyte de-differentiation and loss of HNF4α expression are associated with worsening pathology and impaired liver function [32]. Additionally, Alpha-fetoprotein

(AFP)—a fetal liver marker that is often re-expressed during hepatic injury and regeneration, was significantly decreased in the GEF group (Fig. 5B). Lower AFP suggests less liver injury as there is less stimulus to regenerate. The reduced AFP is also consistent with higher HNF4α as some of AFP positive cells are thought to arise from more mature HNF4α positive hepatocytes that de-differentiate to re-acquire a progenitor-like state [33]. Interestingly, Cyclin E—a critical regulator of the G1/S transition in the cell cycle—levels were upregulated (Fig. 5C). Elevated Cyclin E transcript levels suggest increased hepatocyte proliferation, potentially contributing to tissue renewal and functional recovery [34].

To directly assess the pro-proliferative effects of GEF on hepatocytes, we performed an *in vitro* proliferation assay using AML12 cells—a healthy murine hepatocyte cell line. Cells incubated with GEF exhibited significantly greater proliferation over a 48-hour period compared to PBS-treated controls (Fig. 5D). This finding corroborates the gene expression data and indicates that GEF can stimulate hepatocyte growth in a non-inflammatory, regenerative context. Taken together, these results point to benefits of GEF treatment in the promotion of liver repair and regeneration. By activating cell cycle genes, and enhancing the expression hepatocyte identity markers, GEF appears to support not only the resolution of injury but also the recovery of functional liver tissue.

To complement our molecular and functional analyses, we performed histological evaluation of liver tissues to directly visualize the effects of GEF treatment on hepatocyte proliferation and lipid accumulation. Ki67 immunohistochemical staining was used to assess hepatocyte proliferation in situ. Representative liver sections from GEF-treated mice (Fig. 6B) showed a markedly increased number of Ki67-positive nuclei compared to those from saline-treated controls (Fig. 6A). We quantified this increase by counting the positive nuclei in 6 randomly chosen, 20x fields per section for each mouse and then plotting the average number of Ki67-positive nuclei in GEF treated group as compared to the control (Fig. 6C). This significantly increased Ki67-positive nuclei evidence supports our earlier findings of elevated Cyclin E expression and enhanced *in vitro* AML12 proliferation, indicating that GEF promotes active hepatocyte cell cycling and tissue renewal at the cellular level [35, 36]. Importantly, this increase in proliferation occurred in a background of reduced inflammation and fibrosis, suggesting a favorable regenerative rather than pathological proliferation.

To assess hepatic lipid burden, we performed Oil Red O staining, which selectively labels neutral lipids within tissue sections. Liver samples from GEF-treated mice (Fig. 6E) exhibited a notable reduction in lipid content, with visibly fewer and smaller lipid droplets as compared to saline-treated animals (Fig. 6D) that displayed dense and widespread lipid droplet accumulation. To quantify this effect, we calculated the percent neutral lipid positive area by measuring the area occupied by red droplets relative to the total area of the micrograph for each mouse. The average percent neutral lipid positive area for the GEF treated mice was significantly lower as compared to the control group (Fig. 6F). This reduction in hepatic steatosis is consistent with the observed decrease in serum cholesterol and glucose and likely reflects enhanced lipid utilization and decreased hepatic lipogenesis mediated by FGF21 activity in the dual agonist. These histological results provide visual confirmation of the biochemical and molecular improvements induced by GEF therapy.

## Conclusions

In this study, we present the rational design, characterization, and preclinical evaluation of a unimolecular dual agonist—GLP1-ELP-FGF21 (GEF)—that simultaneously activates GLP-1 and FGF21 signaling pathways. By leveraging an ELP linker, the dual agonist was engineered to possess not only receptor-targeted biological activity but also favorable pharmacokinetic properties through its reversible thermal phase behavior. This platform enables a single molecule to deliver multi-hormonal functionality with enhanced systemic stability. In a diet-induced model of advanced MASH with fibrosis, GEF treatment led to significant improvements in body weight, liver mass, and serum metabolic parameters, including cholesterol, insulin, and glucose. At the molecular level, GEF attenuated hepatic inflammation and fibrosis, as evidenced by reduced expression of pro-inflammatory cytokines and fibrotic markers. By simultaneously reducing pro-inflammatory cytokines and fibrogenic mediators at both the gene and protein levels, GEF addresses multiple key drivers of disease progression. Histological and functional analyses further revealed increased hepatocyte proliferation and decreased lipid accumulation in liver tissue, suggesting that GEF not only halts disease progression but actively promotes hepatic regeneration and repair. These results highlight the therapeutic potential of dual GLP-1 and FGF21 activation in reversing liver pathology even at a late stage of disease, and provide a mechanistic rationale for continued development of this unimolecular strategy in chronic liver disease.

Looking forward, further development of GEF will benefit from extended pharmacodynamic studies, dose optimization, and safety profiling in larger animal models. In addition, mechanistic studies in primary human hepatocytes and MASH patient-derived organoids could provide translational insights into receptor dynamics and tissue-specific effects. Ultimately, this unimolecular platform may be adapted to include additional hormone modules or tailored to different disease stages, providing a versatile framework for next-generation therapies targeting multifactorial metabolic disorders.

## Materials and methods

# Expression and Purification of GLP1-ELP-FGF21 Fusion Protein

To produce the final GLP1-ELP-FGF21 construct, the fusion protein MSKGPG-tev-GLP1-ELP-FGF21 was first expressed and purified. The N-terminal MSKGPG leader sequence enhances protein expression yield in *E. coli* [21], and a TEV protease recognition site (tev = ENLYFQG) enables site-specific and seamless cleavage of the leader sequence leaving the GLP-1 active on the N-terminus of the fusion protein. The TEV protease was also recombinantly produced as a $his_6$-ELP-TEV fusion where ELP enabled proper folding of the TEV during expression in *E. coli*, and the histidine (his-6x) tag assisted in purification of the protein from lysate [37–39].

**Expression and Purification of MSKGPG-tev-GLP1-ELP-FGF21**

The plasmid encoding the gene for MSKGPG-tev-GLP1-ELP-FGF21 fusion was transformed into SHuffle T7 Express cells (New England Biolabs), which support enhanced disulfide bond formation in the cytoplasm. The growth media was prepared by supplementing Terrific broth (TB; 55 g/L; VWR) with 0.4% glycerol and 45 μg/mL kanamycin. A 50 mL overnight culture was grown at 37°C with shaking at 250 rpm overnight. This pre-culture was pelleted by centrifugation at 3365 rcf, resuspended in fresh growth media, and used to inoculate three 1-liter cultures in 6-liter Erlenmeyer flasks. Cultures were grown at 30°C, with shaking at 200 rpm in an orbital shaker until an optical density ($OD_{600}$) of ~ 0.5 was reached, at which point protein expression was induced by adding 250 μM isopropyl-β-D-thiogalactopyranoside (IPTG). The temperature was then lowered to 16°C, and cultures were incubated overnight. Cells were harvested by centrifugation at 4000 rcf for 10 min at 4°C, and the pellets were resuspended in ice-cold PBS followed by cell lyses by sonication (QSonica sonicator, Newtown, CT) using 10 s on / 40 s off cycle at 75% amplitude for a total On-time of 3 min. To precipitate nucleic acid contaminants in the lysate, 10% polyethyleneimine (PEI) (Millipore Sigma, Burlington, MA) was added and the lysate was clarified by centrifugation at 23,000 rcf, 4°C for 10 min. The PEI precipitation step was repeated 2–3 additional times until the cold lysate was clear with minimal turbidity. The supernatant was retained for Inverse Transition Cycling (ITC)-based purification, exploiting the phase behavior of ELP [17, 40]. Purification was initiated by raising the temperature of the clarified lysate to 25°C and adding 0.2 M ammonium sulfate ($(NH_4)_2SO_4$; Millipore Sigma) to induce the ELP phase transition. The resulting coacervate suspension was centrifuged at 25°C for 15 min at 23,000 rcf (“hot spin”), and the pellet containing aggregated ELP fusion protein was collected. This pellet was then resuspended in cold PBS and gently rotated overnight at 4°C (R4045 RotoBot Programmable Rotator, Benchmark Scientific, Sayreville, NJ). Insoluble debris was removed by centrifugation at 4°C for 10 min at 23,000 rcf (“cold spin”). This ITC cycle—consisting of salt-induced coacervation, centrifugation at elevated temperature, resolubilization at 4°C, and clarification—was repeated twice more to ensure high purity of the fusion proteins. The final protein preparation was analyzed by SDS-PAGE stained with Coomassie Blue to confirm expected molecular weight and purity.

### Expression and Purification of $(His)_6$-ELP-TEV Protease

The $(His)_6$-ELP-TEV protease was expressed using a similar protocol as GEF, but after harvest, the cells were resuspended in equilibration buffer (EQ = 20 mM Tris-HCl pH 8, 200 mM NaCl, 10 mM imidazole). Lysis was performed by sonication on ice (10 s on / 40 s off, 75% amplitude, 3 min total) followed by centrifugation. The clarified lysate was applied to a HisPur Cobalt Resin (Thermofisher) column equilibrated with EQ buffer for purification by immobilized metal affinity chromatography. The resin was washed once with EQ buffer followed by wash buffer (20 mM Tris-HCl pH 8, 200 mM NaCl, 25 mM imidazole) until no further protein was detected by the absorbance at 280 nm ($A_{280}$). Elution was carried out using 200 mM imidazole in the EQ buffer and the purity of elution fractions were analyzed by SDS-PAGE. The pure fractions were combined and dialyzed into 50 mM Tris–HCl (pH 8.0), 200 mM NaCl, 0.5 mM EDTA for storage at -20°C.

*TEV Cleavage Reaction and Purification of GLP1-ELP-FGF21 (GEF)*: Cleavage of the fusion protein was carried out by mixing MSKGPG-tev-GLP1-ELP-FGF21 with $(His)_6$-ELP-TEV protease in 50 mM Tris–HCl (pH 8.0), 200 mM NaCl, 0.5 mM EDTA, 3 mM glutathione, at a protease to substrate (GEF) molar ratio of ~ 1:12. The reaction was incubated overnight at 4°C with gentle mixing and completion of the reaction was monitored by SDS-PAGE. Post-cleavage, the TEV reaction buffer was exchanged with 20 mM Tris (pH 8) and the mixture containing cleaved GEF and his-ELP-TEV was passed through cobalt resin to obtain pure GEF in the flow through. Final purification was achieved by anion exchange chromatography where the sample was applied to a HiTrap™ Q HP column (Cytiva) equilibrated with 20 mM Tris-HCl (pH 8.0), and elution was performed using a linear gradient up to 50% of a high-salt buffer (20 mM Tris-HCl, 1 M NaCl, pH 8) on an AKTA protein purification system (Cytiva). Peak fractions containing pure GEF were confirmed by SDS-PAGE and $A_{260/280}$ ratio measurements, pooled, concentrated in PBS using ultracentrifugal filtration (30 kDa MWCO Amicon, Millipore Sigma), and stored at − 20°C.

**Endotoxin Removal and Quantification**

To minimize potential immune response in downstream applications, the recombinant GEF was subjected to endotoxin clearance using Acrodisc syringe filters (Pall Corporation, Port Washington, NY). The residual endotoxin levels were quantified using the Endosafe Nexgen-PTS system (Charles River Laboratories, Wilmington, MA) and were below the FDA limit of 5 EU per kg mouse body weight in all GEF samples injected into mice.

**In vitro Characterization of GEF**

**Thermal Phase Behavior**

The protein was resuspended in 1x PBS at 200 µM concentration at 4°C, and a serial dilution in PBS was performed resulting in 200, 50, 25, 12.5 µM as the concentrations to be tested. The optical density (OD) of the solution was monitored at 600 nm as a function of temperature on a temperature-controlled UV-vis spectrophotometer (Cary 300 Bio, Varian instruments). Starting at 20°C, the temperature of the samples in the cuvette was increased at a rate of 0.3°C/min until ~ 48°C and the absorbance data was recorded at each 0.6°C intervals. A sharp increase in the OD with temperature is indicative of the phase transition and the temperature at the inflection point of the optical density is defined as the $T_t$. The OD vs temperature was plotted and the temperature at the inflection point that defines the $T_t$ was determined by finding the maximum of the first derivative of the OD versus temperature using GraphPad Prism software.

**Formation and Reversibility of Coacervate Droplets by Light Microscopy**

The GEF protein was resuspended in PBS at 200 µM. For imaging, a 3 µL drop of the sample was placed on a glass slide with double-sided sticky tape lining the sample area to allow sufficient space for phase separation to occur between the slide and coverslip. The sample was imaged at 20x magnification on a Zeiss microscope (Axio Imager.D2m) with a custom heating insert, at a temperature above the $T_t$ (35°C)

of the fusion protein and the temperature was then decreased to below $T_t$ (25 °) to visualize the reversibility of the phase transition.

*Quantification of GLP-1R Activation by cAMP-Responsive Luciferase Assay*: To determine the activity of GLP-1 in the fusion protein, a HEK293 (RRID: CVCL_0045) cell line stably expressing the GLP-1 receptor and a cAMP-inducible luciferase reporter gene was used. The cell line was confirmed to be contamination free by culturing and passaging them at least two times before starting the assay. For the assay, cells were plated at 1 × $10^5$ cells/cm² in 96-well plates and incubated overnight. In parallel, GEF was pretreated with dipeptidyl peptidase-4 (DPP4, ProSpec-Tany) at a 1:500 molar ratio (DPP4:GLP-1) and incubated overnight at 4°C to cleave the leader peptide and reveal the biologically active N-terminus. The following morning, cell culture media were replaced with an induction buffer containing 129 mM NaCl, 4.8 mM KCl, 1.2 mM $MgSO_4$, 1.2 mM $KH_2PO_4$, 2.5 mM $CaCl_2$, 5 mM $NaHCO_3$, 10 mM HEPES, 0.5% BSA, and 50 µM IBMX (3-isobutyl-1-methylxanthine). Cells were then treated with serial dilutions of GLP-1R agonist for 5 h. After incubation, media were replaced with Bright-Glo luciferase substrate (Promega, Madison, WI), and the luminescence was measured using a Victor X3 plate reader (PerkinElmer). Signals were normalized against vehicle-treated controls, and dose-response curves were fit using GraphPad Prism 8 to calculate $EC_{50}$ values via a three-parameter logistic fit.

*Assessment of FGF21 Bioactivity via ERK1/2 Phosphorylation*: The *in vitro* activity of FGF21 in GEF was evaluated by measuring the phosphorylation of extracellular signal–regulated kinases 1/2 (ERK1/2) in a HEK293 (RRID: CVCL_0045) cell line engineered to stably express murine FGFR1 and β-Klotho [18]. The cell line was confirmed to be contamination free by culturing and passaging them at least two times before starting the assay. For the assay, cells were seeded at a density of 5 × $10^4$ cells/cm² and allowed to adhere overnight. Following a 6-h period of serum deprivation, cells were stimulated with a concentration gradient of either the fusion protein or recombinant mouse FGF21 (ProSpec-Tany, East Brunswick, NJ) for 5 min. Post-treatment, cell lysates were analyzed for levels of phosphorylated and total ERK1/2 using the AlphaLISA SureFire Ultra assay kits (PerkinElmer). Signal quantification was performed with an EnSpire Alpha plate reader (PerkinElmer). Phosphorylated ERK1/2 values were normalized to total ERK1/2, and the resulting dose-response data were analyzed using GraphPad Prism 8 software (GraphPad Software, La Jolla, CA) to derive $EC_{50}$ values via a three-parameter logistic fit.

*Assessment of GEF for Hepatocyte Proliferation*: AML12 (RRID: CVCL_0140) cells—a healthy murine hepatocyte cell line—were purchased from ATCC for the *in vitro* proliferation assay and cultured as per supplier's instructions. For the assay, 90 µL of cell suspension, corresponding to 5 x $10^3$ cells/well, were plated in a 96-well format a day before the assay. Cells were treated with 4 µM of GEF or PBS control in 30 µL media and were incubated for 4, 24, and 48 h. 20 µL of CellTiter 96 AQueous (Promega) reagent was added to each well and incubated for 1 h before measurement of the absorbance at 490 nm. The assay measures the reduction of tetrazolium reagent by metabolically active cells to determine cell viability at each time point after the treatment.

# Therapeutic Efficacy of the GEF in a Model of Advanced MASH

### Animals

24-week adult male C57Bl6/J were purchased from the Jackson laboratory (# 000664, Jackson Laboratory, Bar Harbor, ME) and were maintained in a temperature-controlled, pathogen-free room on 12-h light and dark cycles with ad libitum access to water and diet. All mice (n = 18) were fed a choline-deficient L-amino acid defined high-fat diet (CDA-HFD, A06071302, Research Diet, New Brunswick, NJ) for 16 weeks. The mice received s.c. injection of either vehicle control (PBS, Veh; n = 9) or GEF at a 750 nmol/kg dose (200 μM, GEF; n = 9) once a week for the last 4-weeks. At the start of week 17, mice were euthanized for whole tissue harvest. Slices of liver were formalin-fixed for paraffin embedding, and the remainder were snap frozen in liquid nitrogen for RNA and protein analysis. The blood samples were collected in Microvette 500 (Sarstedt Inc, Newton, NC) following the manufacturer's instructions—centrifuged at 10,000 rcf for 10 min at room temperature and supernatants were transferred to a new tube for analysis. Animal care and diet procedures were conducted in compliance with an approved Duke University IACUC protocol, and those set forth in the "Guide for the Care and Use of Laboratory Animals" as published by the National Research Council.

### Serum Analysis

Measurements in mouse serum for glucose, total cholesterol, HDL-cholesterol, and triglycerides were performed on a Beckman-Coulter DxC 600 clinical analyzer using reagents also from Beckman (Brea, CA). An immunoassay for mouse insulin was run using a kit and QuickPlex imager from Meso Scale Discovery (Rockville, MD).

*qRT-PCR*: Total RNA was extracted from whole liver chips using TRIzol (LifeTechnologies, Carlsbad, CA) according to the manufacturer's instructions. First-strand cDNA was prepared by reverse transcription, using 5 μg of DNA-free RNA as template for the High-Capacity cDNA Reverse Transcription kit (Applied Biosystems). For qRT-PCR, 1% of the first-strand reaction was amplified using the StepOne Plus Real-Time PCR Platform (ABI/Life Technologies) and specific intron-spanning oligonucleotide primers for target sequences, as well as the ribosomal S9 housekeeping gene as reference control. qRT-PCR parameters were as follows: denaturing at 95°C for 3 minutes, followed by 40 cycles of denaturing at 95°C for 10 seconds and annealing/extension at the optimal primer temperature for 60 seconds. Threshold cycles (*C*t) and product melt temperature were automatically calculated by the StepOne Plus Real-Time Detection System. Target gene levels are presented as a ratio to levels detected in the corresponding control tissue or cells according to the ΔΔCt method. Primer sequences are listed in Table 1.

### Protein Quantification by ELISA

For the detection of IL-6, the whole liver tissue was lysed by RIPA buffer with proteinase inhibitor (P8340, Millipore Sigma). The 40 μg of lysate protein was detected for IL-6 protein by IL-6 ELISA kit (KMC0061,

Life tech., Frederick, MD) following the manufacturer's instructions.

*Immunohistochemistry and Quantitation*: Liver tissues were fresh frozen or fixed in formalin and embedded in paraffin blocks using standard methods. Lipid accumulation in liver was evaluated by Oil Red O (Cat# O0625-25G, Sigma-Aldrich, St. Louis, MO). Briefly, fresh tissue samples were fixed with 10% formalin, stained with Oil Red O (10 min), and counterstained with hematoxylin (2 min). Results were examined by light microscopy. Immunohistochemistry was used to detect the target proteins using the following antibodies: Rabbit-anti-Ki67 (ab16667, Abcam, Cambridge, MA). Secondary antibodies were HRP-conjugated anti-rabbit (K4003, Agilent, Santa Clara, CA). Blocking and chromogenic detection were performed using the Envision System (Agilent) according to the manufacturer's protocol, with DAB substrate (K3466, Agilent). Tissue sections were counterstained with Harris Hematoxylin (Leica, Richmond, IL). Negative controls included liver specimens exposed to 1% bovine serum albumin instead of the respective primary antibodies. The numbers of Ki67 immuno-reactive nuclei were quantified by counting 6 randomly chosen, 20x fields per section per mouse.

## Statistics

All data is expressed as mean ± SEM. Statistical analysis was performed using Student's *t*-test as indicated. Differences with $p \leq 0.05$ were considered statistically significant.

Table 1
Primer sequences

| Gene Name | Sequence |
|---|---|
| TGF-β | 5'-TTG CCC TCT ACA ACC AAC ACA A |
| | 5'-GGC TTG CGA CCC ACG TAG TA |
| TNF-α | 5'-CGT CAG CCG ATT TGC TAT CT |
| | 5'-CGG ACT CCG CAA AGT CTA AG |
| IL-6 | 5'-GAG CCC ACC AAG AAC GAT AG |
| | 5'-TCC ACG ATT TCC CAG AGA AC |
| Il-18 | 5'-CAG GCC TGA CAT CTT CTG CAA |
| | 5'-TCT GAC ATG GCA GCC ATT GT |
| IL-33 | 5'-TCC ACG GGA TTC TAG GAA GA |
| | 5'-GAG GCA GGA GAC TGT GTT AAA |
| HIF-1α | 5'-CTC ATC CAA GGA GCC TTA ACC |
| | 5'-TTC GCT TCC TCT GAG CAT TC |
| HNF4 α | 5'-TCA ACG ACC GGC AGT ACG AC |
| | 5'-CTG GCA GAC CCT CCG AGA AG |
| AFP | 5'-CCG AGG AGG AAG TGA ACA AA |
| | 5'-GGC TTT CTA AAC ACC CAT CG |
| Cyc E | 5'-CAG AGC AGC GAG CAG GAG C |
| | 5'-GCA GCT GCT TCC ACA CCA CT |
| S9 | 5'-GGG CCT GAA GAT TGA GGA TT |
| | 5'-CGG GCA TGG TGA ATA GAT TT |

## Declarations

# Acknowledgements

The HEK293 cell line used for the GLP-1 activity assay was originally a gift from T. Kieffer at the University of British Columbia and the HEK293 cell line used for FGF21 activity assay was developed by Dr. Caslin Gilroy in the Chilkoti lab. Authors thank Duke Substrate Services Core and Research Support (SSCRS) Histology Core Lab for their assistance with slides preparation for histological analyses.

Authors also thank Dr. Mike Muehlbauer from Duke Molecular Physiology Institute for overseeing the serum analysis.

## References

1. Younossi, Z.M., et al., *Global epidemiology of nonalcohoic fatty liver disease-Meta-analytic assessment of prevalence, incidence, and outcomes*. Hepatology, 2016. 64(1): p. 73–84.
2. Armstrong, M.J., et al., *Liraglutide safety and efficacy in patients with non-alcoholic steatohepatitis (LEAN): a multicentre, double-blind, randomised, placebo-controlled phase 2 study*. Lancet, 2016. 387(10019): p. 679–690.
3. Harrison, S.A., et al., *A Phase 3, Randomized, Controlled Trial of Resmetirom in NASH with Liver Fibrosis*. N Engl J Med, 2024. 390(6): p. 497–509.
4. Ravela, N., et al., *Early experience with resmetirom to treat metabolic dysfunction-associated steatohepatitis with fibrosis in a real-world setting*. Hepatol Commun, 2025. 9(4).
5. Petroni, M.L., F. Perazza, and G. Marchesini, *Breakthrough in the Treatment of Metabolic Associated Steatotic Liver Disease: Is it all over?* Dig Liver Dis, 2024. 56(9): p. 1442–1451.
6. Newsome, P.N., et al., *A Placebo-Controlled Trial of Subcutaneous Semaglutide in Nonalcoholic Steatohepatitis*. N Engl J Med, 2021. 384(12): p. 1113–1124.
7. Amiram, M., et al., *Injectable protease-operated depots of glucagon-like peptide-1 provide extended and tunable glucose control*. Proc Natl Acad Sci U S A, 2013. 110(8): p. 2792–7.
8. Liu, Y., et al., *Fibroblast growth factor 21 deficiency exacerbates chronic alcohol-induced hepatic steatosis and injury*. Sci Rep, 2016. 6: p. 31026.
9. Tillman, E.J. and T. Rolph, *FGF21: An Emerging Therapeutic Target for Non-Alcoholic Steatohepatitis and Related Metabolic Diseases*. Front Endocrinol (Lausanne), 2020. 11: p. 601290.
10. Harrison, S.A., et al., *Efruxifermin in non-alcoholic steatohepatitis: a randomized, double-blind, placebo-controlled, phase 2a trial*. Nat Med, 2021. 27(7): p. 1262–1271.
11. Talukdar, S., et al., *A Long-Acting FGF21 Molecule, PF-05231023, Decreases Body Weight and Improves Lipid Profile in Non-human Primates and Type 2 Diabetic Subjects*. Cell Metab, 2016. 23(3): p. 427–40.
12. Pan, Q., et al., *A novel GLP-1 and FGF21 dual agonist has therapeutic potential for diabetes and non-alcoholic steatohepatitis*. EBioMedicine, 2021. 63: p. 103202.
13. Gilroy, C.A., et al., *Sustained release of a GLP-1 and FGF21 dual agonist from an injectable depot protects mice from obesity and hyperglycemia*. Sci Adv, 2020. 6(35): p. eaaz9890.
14. Hassouneh, W., S.R. MacEwan, and A. Chilkoti, *Fusions of elastin-like polypeptides to pharmaceutical proteins*. Methods Enzymol, 2012. 502: p. 215–37.
15. Amiram, M., et al., *A depot-forming glucagon-like peptide-1 fusion protein reduces blood glucose for five days with a single injection*. J Control Release, 2013. 172(1): p. 144–151.

16. Luginbuhl, K.M., et al., *One-week glucose control via zero-order release kinetics from an injectable depot of glucagon-like peptide-1 fused to a thermosensitive biopolymer*. Nat Biomed Eng, 2017. 1.
17. Meyer, D.E. and A. Chilkoti, *Purification of recombinant proteins by fusion with thermally-responsive polypeptides*. Nat Biotechnol, 1999. 17(11): p. 1112–5.
18. Gilroy, C.A., S. Roberts, and A. Chilkoti, *Fusion of fibroblast growth factor 21 to a thermally responsive biopolymer forms an injectable depot with sustained anti-diabetic action*. J Control Release, 2018. 277: p. 154–164.
19. Hebbard, L. and J. George, *Animal models of nonalcoholic fatty liver disease*. Nat Rev Gastroenterol Hepatol, 2011. 8(1): p. 35–44.
20. Matsumoto, M., et al., *An improved mouse model that rapidly develops fibrosis in non-alcoholic steatohepatitis*. Int J Exp Pathol, 2013. 94(2): p. 93–103.
21. McDaniel, J.R., et al., *Recursive directional ligation by plasmid reconstruction allows rapid and seamless cloning of oligomeric genes*. Biomacromolecules, 2010. 11(4): p. 944–52.
22. Gilroy, C.A., *Controlled Release Systems for Treating Type 2 Diabetes and Their Application toward Multi-Agonist Combination Therapies.* Doctoral dissertation, Duke University, 2019.
23. Kapust, R.B., et al., *Tobacco etch virus protease: mechanism of autolysis and rational design of stable mutants with wild-type catalytic proficiency*. Protein Eng, 2001. 14(12): p. 993–1000.
24. Elmansi, A.M., et al., *What doesn't kill you makes you stranger: Dipeptidyl peptidase-4 (CD26) proteolysis differentially modulates the activity of many peptide hormones and cytokines generating novel cryptic bioactive ligands*. Pharmacol Ther, 2019. 198: p. 90–108.
25. Mackay, J.A., et al., *Quantitative model of the phase behavior of recombinant pH-responsive elastin-like polypeptides*. Biomacromolecules, 2010. 11(11): p. 2873–9.
26. Ozer, I., et al., *An injectable PEG-like conjugate forms a subcutaneous depot and enables sustained delivery of a peptide drug*. Biomaterials, 2023. 294: p. 121985.
27. Barrera, J.G., et al., *GLP-1 and energy balance: an integrated model of short-term and long-term control*. Nat Rev Endocrinol, 2011. 7(9): p. 507–16.
28. Nagao, M., et al., *Cardioprotective Effects of High-Density Lipoprotein Beyond its Anti-Atherogenic Action*. J Atheroscler Thromb, 2018. 25(10): p. 985–993.
29. Wang, Z., et al., *Macrophage in liver Fibrosis: Identities and mechanisms*. Int Immunopharmacol, 2023. 120: p. 110357.
30. Koyama, Y. and D.A. Brenner, *Liver inflammation and fibrosis*. J Clin Invest, 2017. 127(1): p. 55–64.
31. Cai, S.H., et al., *Increased expression of hepatocyte nuclear factor 4 alpha transcribed by promoter 2 indicates a poor prognosis in hepatocellular carcinoma*. Therap Adv Gastroenterol, 2017. 10(10): p. 761–771.
32. Kotulkar, M., et al., *Role of HNF4alpha-cMyc Interaction in CDE Diet-Induced Liver Injury and Regeneration*. Am J Pathol, 2024. 194(7): p. 1218–1229.

33. Unzu, C., et al., *Pharmacological Induction of a Progenitor State for the Efficient Expansion of Primary Human Hepatocytes*. Hepatology, 2019. 69(5): p. 2214–2231.
34. Walesky, C. and U. Apte, *Role of hepatocyte nuclear factor 4alpha (HNF4alpha) in cell proliferation and cancer*. Gene Expr, 2015. 16(3): p. 101–8.
35. Williams, C.M., et al., *Monomeric/dimeric forms of Fgf15/FGF19 show differential activity in hepatocyte proliferation and metabolic function*. FASEB J, 2021. 35(2): p. e21286.
36. Kim, S.J., et al., *Regeneration of Non-Alcoholic Fatty Liver Cells Using Chimeric FGF21/HGFR: A Novel Therapeutic Approach*. Int J Mol Sci, 2024. 25(6).
37. Tropea, J.E., S. Cherry, and D.S. Waugh, *Expression and purification of soluble His(6)-tagged TEV protease*. Methods Mol Biol, 2009. 498: p. 297–307.
38. Tang, N.C., et al., *Synthetic intrinsically disordered protein fusion tags that enhance protein solubility*. Nat Commun, 2024. 15(1): p. 3727.
39. Ozer, I., et al., *Polyethylene Glycol-Like Brush Polymer Conjugate of a Protein Drug Does Not Induce an Antipolymer Immune Response and Has Enhanced Pharmacokinetics than Its Polyethylene Glycol Counterpart*. Adv Sci (Weinh), 2022. 9(11): p. e2103672.
40. Hassouneh, W., T. Christensen, and A. Chilkoti, *Elastin-like polypeptides as a purification tag for recombinant proteins.* Curr Protoc Protein Sci, 2010. Chapter 6: p. 6 11 1–6 11 16.

# Figures

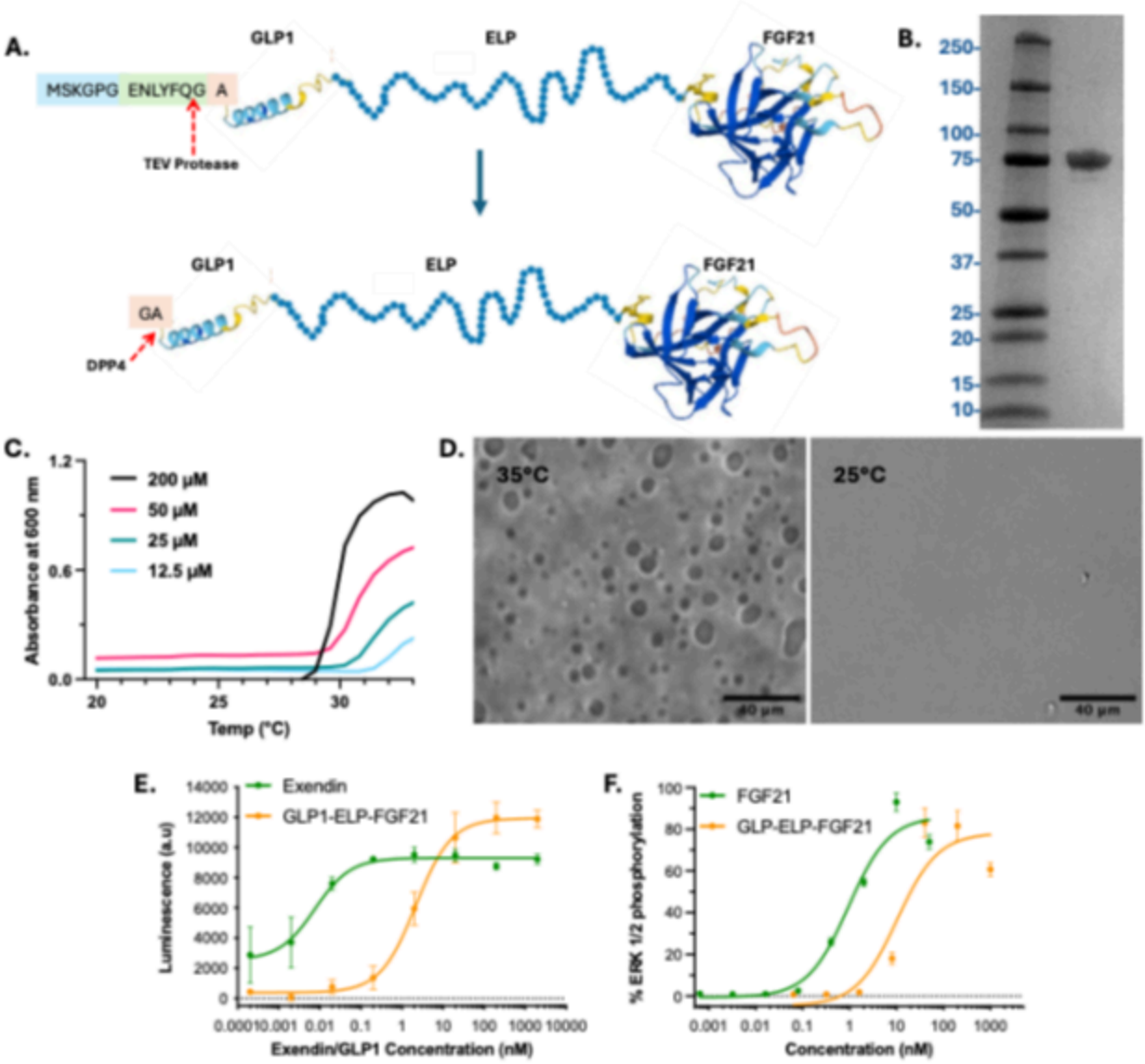



**Figure 1**

Production and *in vitro* characterization of the unimolecular GLP1-ELP-FGF21 (GEF) dual agonist. A) Schematics of the fusion protein with a leader sequence at N-terminus for better translation yield, which is then cleaved-off using TEV Protease to produce the final fusion protein composed of active GLP-1 at the N-terminus and FGF21 at the C-terminus. B) SDS-PAGE gel showing purified final 72 kDa GEF protein. C) Thermal phase behavior of GEF examined by recording absorbance of the protein while heating it at a fixed rate. The sharp increase in absorbance on the heating curve shows transition temperature ($T_t$) of the fusion protein which is inversely proportional to the protein concentration. D) Micrograph of GEF above its $T_t$ showing protein liquid droplets (left) that dissolves on cooling the protein below its $T_t$ (right). This is visual representation for the reversible phase transition behavior of GEF. E-F) GEF functions through both the GLP-1R and FGF21R/b-klotho pathways *in vitro*. E) GLP-1 activity of the GEF was quantified by measuring cAMP production in HEK293 cells stably expressing the GLP-1R and the cAMP-inducible luciferase reporter. A potent GLP-1R agonist—Exendin-4—was used as a positive control for this *in vitro* assay. F) FGF21 activity of GEF was quantified by measuring ERK1/2 phosphorylation in

HEK293 cells stably expressing FGFR1& b-klotho, and by normalizing phospho-ERK1/2 to total ERK1/2. Commercially available mouse FGF21 was used as the positive control. Data is presented as Mean ± SEM, n = 3.

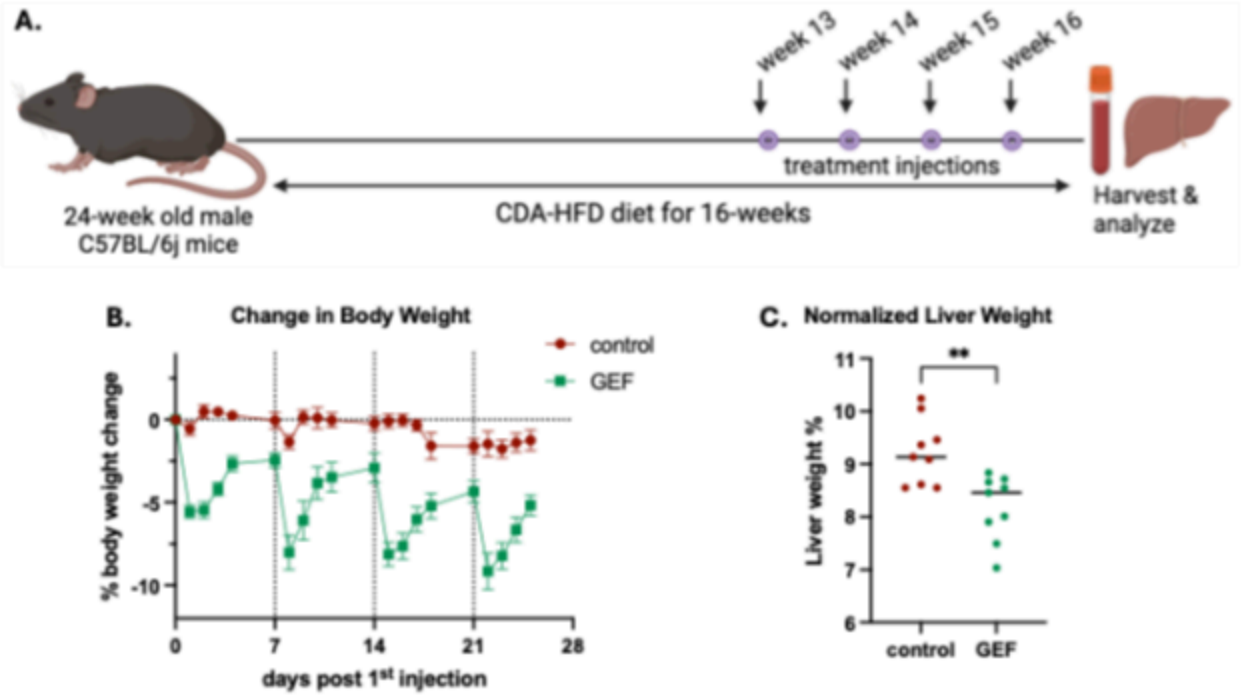



**Figure 2**

*In vivo*experimental design and effects of the dual agonist treatment on body weight and liver weight of the mice. A) 24-week-old C57Bl6/J mice were fed CDA-HFD diet for a total 16-weeks and after 12-weeks, mice were injected s.c. with either GEF at 750 nmol/kg dose or saline as a negative control (n = 9), weekly for four weeks. Body weight was measured daily, and mice were euthanized to harvest their liver and serum after 16-weeks (figure created in BioRender). B) Percent change in body weight after treatment, which was calculated for each mouse in comparison to its body weight the day before treatment started. Data is presented as mean ± SEM for each treatment group. C) Percent liver weight normalized to the body weight of the mouse on the day of euthanization. Each data point represents an individual mouse in each group. Data was analyzed for statistical significance with an unpaired t-test. **P < 0.01.

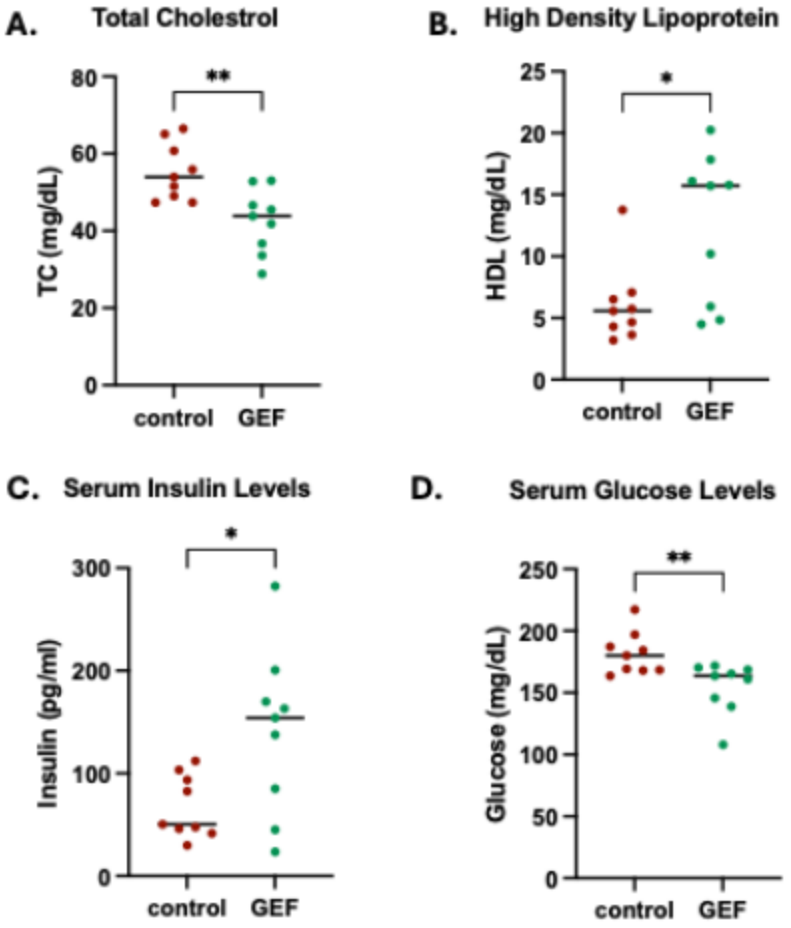



**Figure 3**

End point serum analysis revealed benefits of the dual agonist in improving metabolic parameters. A) total cholesterol, B) HDL, C) insulin, and D) glucose levels in serum. Each data point represents an individual mouse in each group. Data was analyzed for statistical significance with an unpaired t test. *P < 0.05, **P < 0.01.

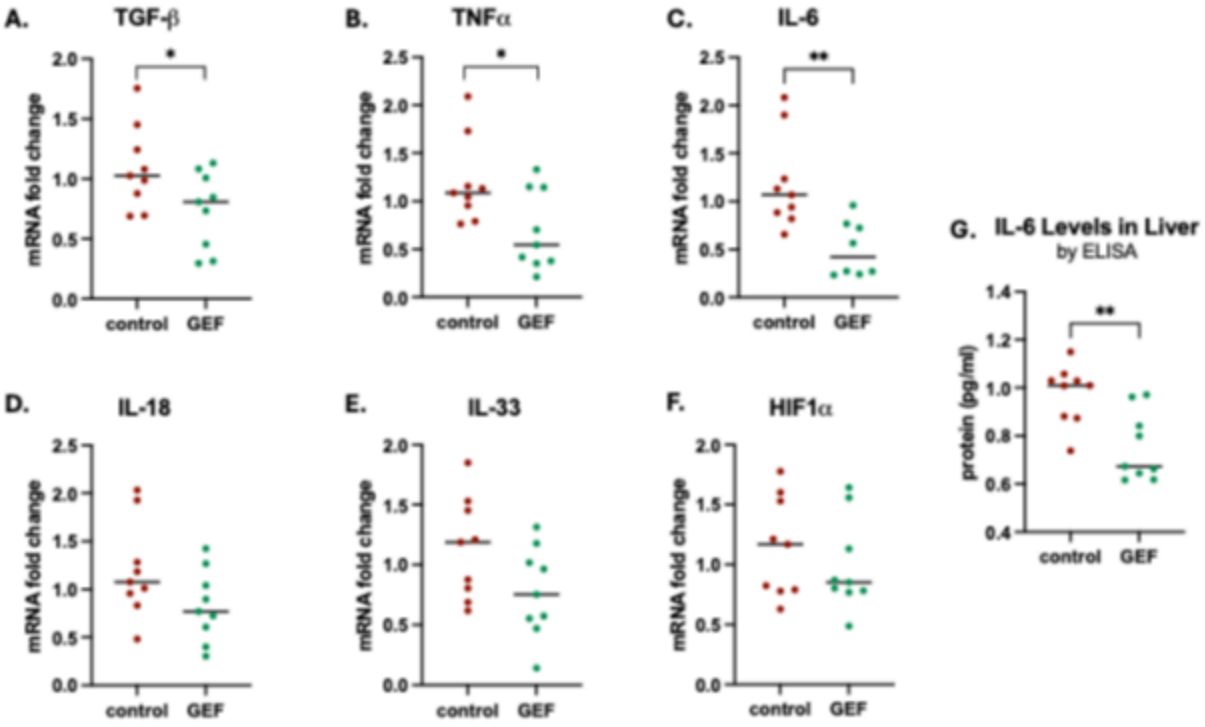



**Figure 4**

Liver analysis by RT-PCR and ELISA revealed benefits of the dual agonist in reducing liver fibrosis and inflammation. A-F) mRNA levels of A) TGF-b, B) TNFa, C) IL-6, D) IL-18, E) IL-33, and F) HIF1a in comparison to the ribosomal S9 housekeeping gene as reference control. G) IL-6 protein levels in liver as determined by ELISA. Each data point represents an individual mouse in each group and data was analyzed for statistical significance with an unpaired t test. *P < 0.05, **P < 0.01.

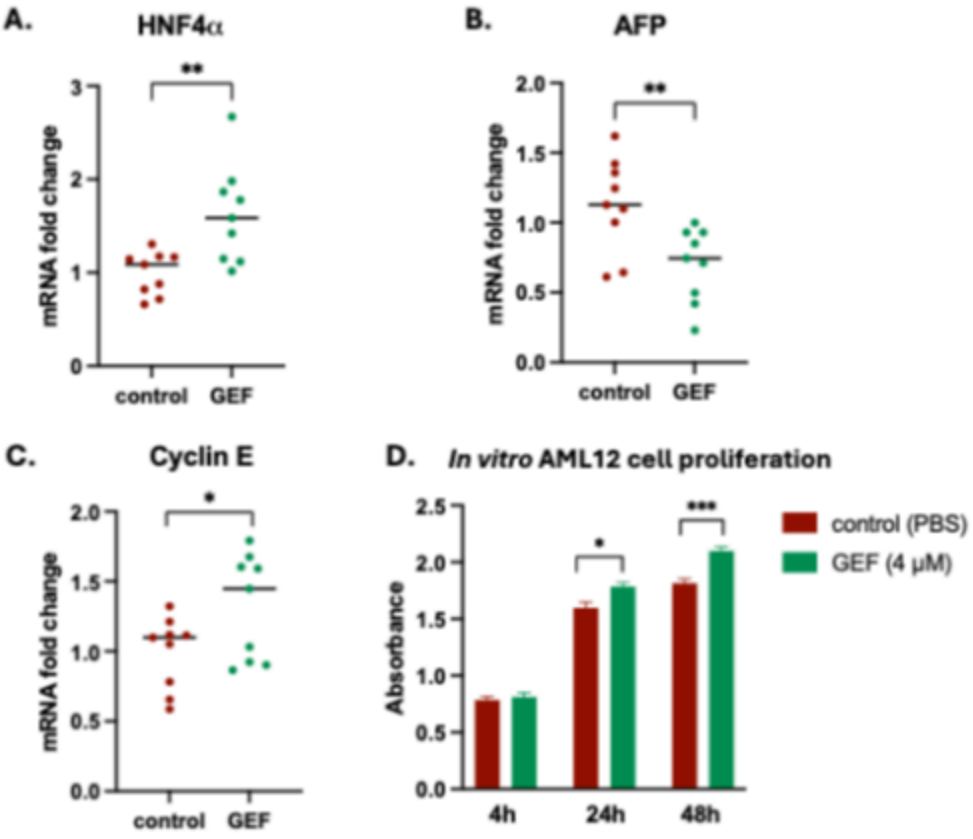



**Figure 5**

Benefits of the dual agonist on overall liver health and *in vitro* healthy hepatocyte proliferation. A-C) mRNA levels of A) HNF4a, B) AFP, and C) Cyclin E in comparison to the ribosomal S9 housekeeping gene as reference control. Each data point represents an individual mouse in each group. D) *in vitro* cell proliferation of AML12 cells over the course of 48 h after incubation with GEF or negative control PBS. Data was analyzed for statistical significance with an unpaired t-test. *P < 0.05, **P < 0.01, ***P < 0.001.

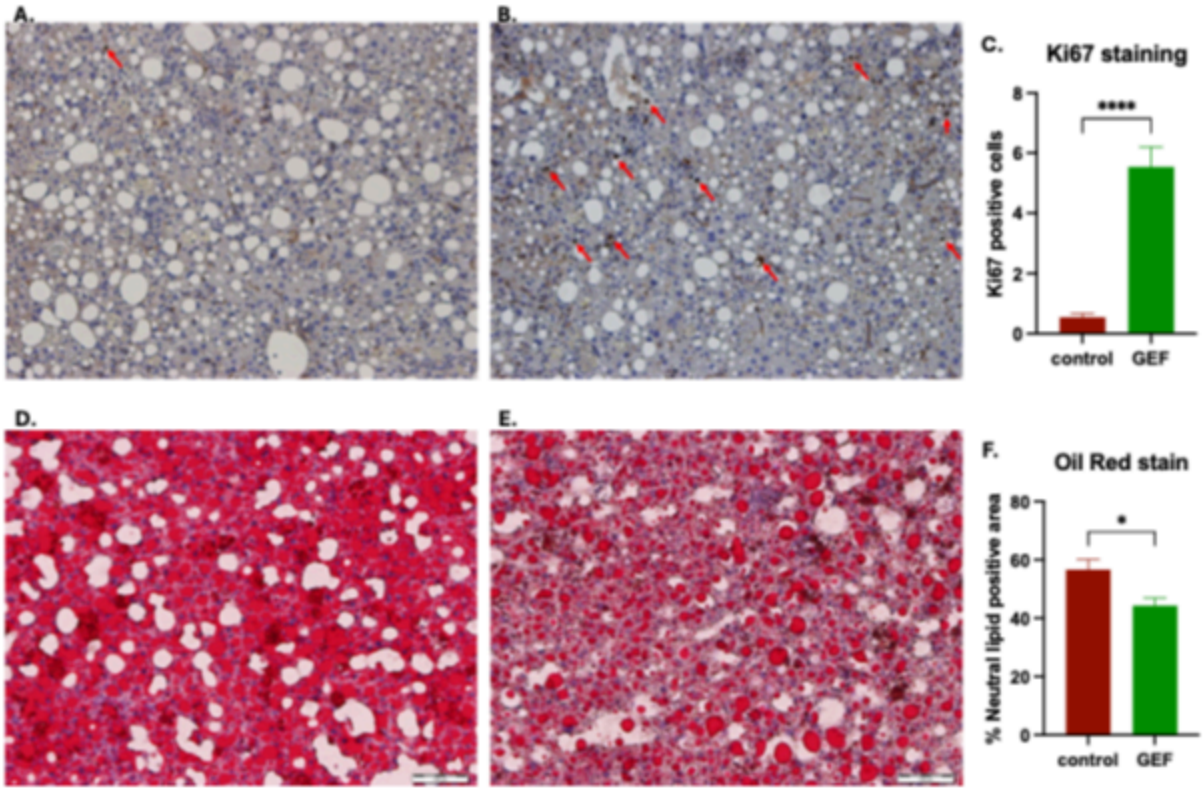



**Figure 6**

Liver tissue histology revealed benefits of the dual agonist in improving hepatocyte proliferation and reducing lipid accumulation in the liver. Ki67 stained micrograph of A) control, and B) GEF. C) Average number of Ki67 positive cells in GEF treated group as compared to the saline control. Oil red stained micrograph of D) control, and E) GEF. F) Averaged percent neutral lipid positive area in GEF treated group as compared to the saline control. Histology results were quantified from 6 randomly chosen, 20x fields per section for each mouse and data is plotted as Mean ± SEM. Data was analyzed for statistical significance with an unpaired t test. *P < 0.05, ****P < 0.0001.